THE ASTROPHYSICAL JOURNAL, 383:L81–L84, 1991 December 20

APERTURE SYNTHESIS CS(2–1) OBSERVATIONS OF A YOUNG STELLAR OBJECT GL 490: ACCRETION FLOW IN GAS DISK

AKIKO NAKAMURA,[1] RYOHEI KAWABE,[2] YOSHIMI KITAMURA,[3] MASATO ISHIGURO,[2]
YASUHIRO MURATA,[2] AND NAGAYOSHI OHASHI[2]
Received 1991 July 24; accepted 1991 October 7

ABSTRACT

We have performed aperture synthesis CS($J = 2$–1) observations of the disk structure of the dense molecular gas around a young stellar object GL 490 with 4″ resolution using the Nobeyama Millimeter Array (NMA). We have found the gas to have a noncircular velocity of $\sim$(1–1.5) km s^{-1}/sin i (i = inclination angle of the disk) and a mass of $\sim 10\ M_\odot$ inside an 8500 AU region of the disk. According to the disk orientation indicated from one-sided cone-shaped optical and IR nebulocities, and the bipolar CO outflow, the noncircular motion is interpreted as inflow. The accretion time scale of the gas τ_{acc} is estimated to be $\sim 3 \times 10^4$ yr and the mass accretion rate $\dot{M}$ to be $\sim 3 \times 10^{-4}\ M_\odot$ yr^{-1}. This would be the first time that a large-scale gas infall in a *disk structure* around a young stellar object was detected.

Subject headings: interstellar: molecules — infrared: sources — stars: formation — stars: individual (GL 490)

1. INTRODUCTION

Information about the process of star formation increased very rapidly during the past two decades with millimeter-wave and infrared observations. However, gas accretion phenomena associated with protostars have been poorly known. For low-mass protostars, the gas accretion rate and velocity of accretion flow is too small to be detected with millimeter-wave observations. Moderate- and high-mass protostars evolve more quickly, so that their lifetime is short compared to low-mass protostars. Large-scale accretion flow of molecular gas onto cloud cores and newly formed stars (possibly stars at a post–ZAMS stage) was found in G10.6−0.4 by the observations of NH_3 absorption lines (Ho & Haschick 1986). Spectroscopic evidence for infall in young stellar objects was obtained by Walker et al. (1986). However, accretion flow onto protostars has not yet been directly detected.

A luminous infrared source GL 490 is one of many young stellar objects embedded in dense molecular cloud cores (Harvey et al. 1979; Lada & Harvey 1981). The dense cloud associated with GL 490 was found to be compact and elongated in the direction orthogonal to the CO flow axis (Kawabe et al. 1984, 1987; Mundy & Adelman 1988; Chini, Henning, & Pfau 1991), and it was suggested that the cloud has a disk structure of dense molecular gas continued to an inner $\sim$1000 AU dust disk inferred from optical and near-infrared observations (Campbell, Persson, & McGregor 1986; Persson, McGregor, & Campbell 1988; Yamashita et al. 1989). Although clear rotational motion was not found, a part of the disklike dense molecular gas shows expansion. We have performed aperture synthesis CS(2–1) observations of GL 490 with the Nobeyama Millimeter Array in order to investigate the velocity structure of the inner part of the disk structure. In this *Letter*, we present the first evidence for accretion flow in the disk and discuss its physical properties.

[1] Department of Physics, Kyoto University, Sakyo-ku Kyoto 606-01, Japan.
[2] Nobeyama Radio Observatory, National Astronomical Observatory, Nobeyama, Minamisaku, Nagano 384-13, Japan.
[3] Department of Liberal Arts, School of Allied Medical Sciences, Kagoshima University, 1208-1, Usuki-cho, Kagoshima 890, Japan.

2. OBSERVATIONS

The CS $J = 2$–1 and 98 GHz continuum emissions from the GL 490 region were observed with the Nobeyama Millimeter Array in 1990 January and March. SIS receivers were used, and their system noise temperatures at the zenith were around 300 K (SSB). An FFT spectrocorrelator (FX) with 1024 velocity channels per baseline (Chikada et al. 1987) was used. The bandwidth was 320 MHz for CS(2–1), giving the velocity resolution of $\sim$1 km s^{-1}. Line-free channels were used for mapping of continuum emission. The field center for the observations was at the position of the infrared source: R.A.(1950) = $03^h23^m38^s.8$, decl.(1950) = 58°36′39″.0 (Joyce et al. 1977). Observations were made by three configurations (total 30 baselines), where the minimum and maximum projected baseline lengths were 15 and 300 m, respectively. Our observations were insensitive to the structures extended more than $\sim$40″. Maps of both the CS(2–1) and the continuum emissions were constructed with a resolution of 3″.3 × 5″.5 (P.A. = 98°). Both bandpass calibration and flux calibration were carried out in the usual manner (e.g., Ishizuki et al. 1990). The absolute positional accuracy in the maps is estimated to be better than 1″, and the uncertainty of their flux scale is $\sim$15%. Maps were made using the CLEAN algorithm in NRAO AIPS. The rms noise level in the continuum was 5.5 mJy beam^{-1} (0.08 K), and that in each CS(2–1) channel map with a 1 km s^{-1} wide was 1.7 K.

3. RESULTS

3.1. CS($J = 2$–1) *Emission*

CS(2–1) line emission was detected at velocities from $V_{LSR} = -10.0$ to -17.7 km s^{-1}. The peak line flux density in our 1 km s^{-1} resolution maps was 1.14 Jy beam^{-1} at $V_{LSR} = -13.4$ km s^{-1} ($\Delta V = 1$ km s^{-1}), which corresponds to 17 K brightness temperature in the 3″.3 × 5″.5 synthesized beam. The total flux density integrated over the above velocity range was 57($\pm$8) Jy km s^{-1}, which corresponds to the $\sim$30% of that detected by a single-dish (Kawabe et al. 1987).

Figure 1 is an integrated intensity map for the velocity range of $V_{LSR} = -12.0$ to -15.8 km s^{-1}. The CS(2–1) emission feature shows an elongated disklike structure with a size of

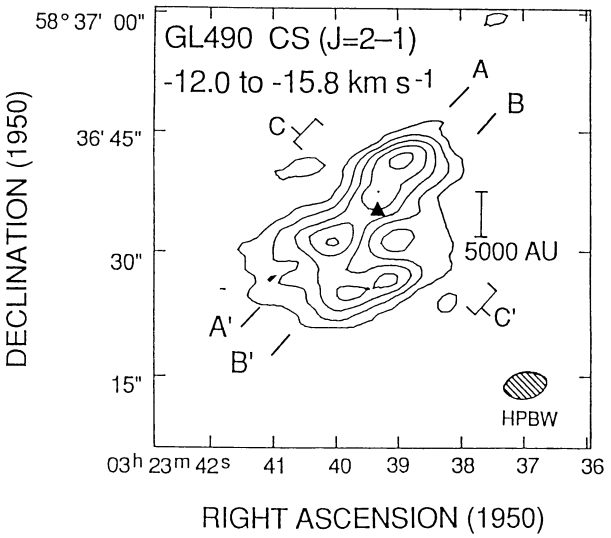

FIG. 1.—Map of the distribution of integrated intensities of the CS(2–1) emission over the velocity range of $V_{LSR} = -12.0$ to -15.8 km s^{-1} around GL 490. The lowest contour is 3 σ level, and the contours are spaced by 2 σ. The beam size is indicated by a hatched ellipse. The filled triangle marks the position of the 98 GHz continuum emission. A linear scale of 5000 AU is shown assuming a distance of 900 pc.

$\sim$(15″–20″) × 30″ centered at the position of a continuum emission (hereafter referred as "center") discussed later. Note that two peaks separated by 13″ are located symmetrically about the center in the disklike feature. The overall structure is similar to both the CS($J = 1$–0) emission feature of $V_{LSR} = -12.5$ to -14.5 km s^{-1} extended 30″ × 60″ (Kawabe et al. 1984), and the ^{13}CO($J = 1$–0) emission feature of $V_{LSR} = -11.1$ to -16.6 km s^{-1} extended 15″ × 50″ (Mundy & Adelman 1988). The position angle of the major axis of the disk is 137° (±5°), almost perpendicular to the orientation of high-velocity CO($J = 1$–0) blue wing (P.A. = 215°) and red wing (P.A. = 35°) (Snell et al. 1984).

Figure 2 shows position-velocity maps along two cuts, A–A′ and B–B′ (shown in Fig. 1) symmetrically separated from the center by 2″.4. The cuts are parallel to the elongation of the disk. A main feature in the maps is complementary arcs. The cut in the northeast (NE; A–A′) shows redshifted velocity, while the other in the southwest (SW; B–B′) shows blueshifted velocity. The two arcs are traced by dashed curves of a model calculation (see § 4.1). The arclike feature inclines overall, and the central parts of the arcs form an oval pattern with an extent of $\sim$19″ × (2–3) km s^{-1} which is almost symmetric with respect to the center. The linear size corresponding to the angular size is 17,000 AU assuming a distance of 900 pc (Harvey et al. 1979).

A position-velocity map along a cut (C–C′ as shown in Fig. 1) perpendicular to the elongation is shown in Figure 3. A prominent feature is a symmetrical velocity structure centered almost on the (0 km s^{-1}, 0″) position in Figure 3, which is composed of two central peaks and redshifted NE and blueshifted SW extensions. The redshifted peak is shifted by 2″ NE and 2 km s^{-1} in velocity relative to the blueshifted peak. The NE and the SW extensions have a size of 10″–15″. It is noted that the SW part of the CS disk structure is blueshifted overall relative to the NE part.

3.2. *Continuum Emission*

The total source flux density at 98 GHz of 280(±50) mJy is obtained, which is consistent with the total flux density of 280 mJy obtained at 110 GHz on account of these flux uncertainties and a spectral index (ν^{α}) of $\alpha = 3$–4 (Mundy & Adelman 1988; Woody et al. 1989). The emission feature is centered southeast to the infrared source. A source position of R.A.(1950) = 03^{h}23^{m}39^s.33(±0^s.05), decl.(1950) = 58°36′35″.2 (±0″.1) was obtained. The position is precisely coincident with

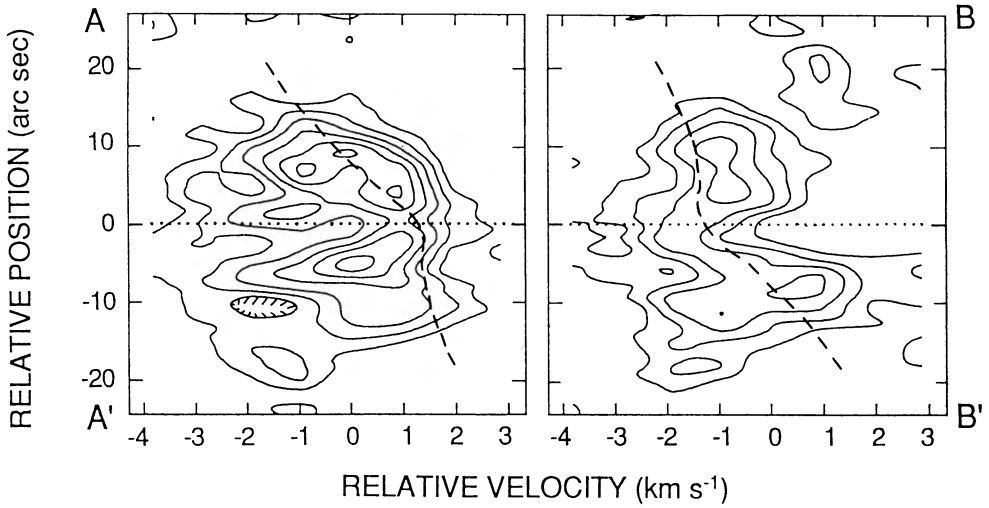

FIG. 2.—Position-velocity maps of CS(2–1) emission toward GL 490 along two parallel cuts shown in Fig. 1, which are separated from the continuum position (center) by 2″.4. The ambient velocity is -13.4 km s^{-1}. Dashed curves are calculated by a simple model where we assumed an infall of a constant velocity with a rigid rotation in an inclined thin disk. Projected velocity V km s^{-1} versus position y (in unit of arcseconds) along A–A′ or B–B′ becomes

$$V = \left[\frac{(x/\cos i) V_{\rm infall}}{\sqrt{y^2 + (x/\cos i)^2}} - y\omega_{\rm rot} \right] \sin i \, ,$$

where we assumed the inclination angle $i = 60°$, the infall velocity $V_{\rm infall} = 1.5$ km s^{-1}, the angular velocity $\omega_{\rm rot} = 1$ km s^{-1}/9″.5, projected separation of A–A′ or B–B′ from the center $x = \pm 2''.4$. Contour interval is 1.5 σ.

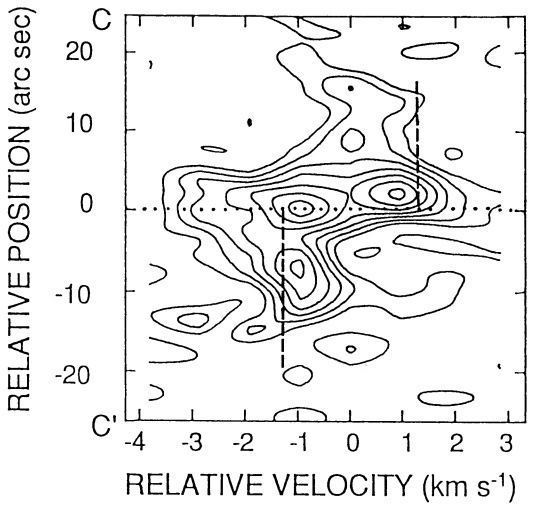

FIG. 3.—Position-velocity map of CS(2–1) emission toward GL 490 along a cut perpendicular to the elongation of the disk. The cut C–C′ passes through the center as shown in Fig. 1. Dashed line indicates the position-velocity curve along the C–C′ cut based on the model velocity structure described in Fig. 2. We adopt a constant infall velocity for simplicity; however, the velocity of the gas tends to decrease as leaving the center. Contour interval is 1.5 σ.

a high-resolution (2″.2 × 2″.1) observational result by Mundy & Adelman (1988) at 110 GHz.

4. DISCUSSION

4.1. *Orientation and Velocity Structure of the Disk*

We first present the probable configuration of the gas disk based on the other observations, and then discuss velocity structures in accord with the configuration and the position-velocity maps.

Although we detected a flattened disk, the disk cannot be perfectly edge-on, because the high-velocity molecular outflow consists of both red and blue lobes at scale of ~0.3 pc. An optical and near-infrared reflection nebula has been observed only at the side of the blue lobe at scale of ~0.1 pc (Campbell et al. 1986; Yamashita et al. 1989), which indicates the presence of an obscuring disk. Since the blue lobe of the molecular outflow and the reflection nebula is located at the SW of the center, the near side of the disk is inclined to the NE and the far side to the SW.

Suppose the orientation of the disk to be as described above, the inclination angle of the disk from face-on configuration is roughly estimated from the ratio of the minor and the major axes of the projected disk. From Figure 1,

$$i \sim \cos^{-1} \frac{15''\text{–}20''}{30''} = 60°\text{–}48° . \quad (1)$$

The inclined arcs and the central oval pattern in Figure 2 indicate the existence of a radial motion in addition to a rotational motion. If the rotational axis of the disk roughly coincides with the position-velocity cut shown in Figure 3, which is perpendicular to the disk plane, the velocity structure is reflected only by the radial motion, not by the rotational motion. The radial motion detected in the *flattened* disk structure suggests the motion is inward or outward *along the disk plane.* Figures 2 and 3 indicate that the NE part of the disk has a redshifted velocity and the SW part has a blueshifted velocity. Assuming the above disk configuration, the red NE part of the disk is near side and the blue SW is far side; therefore, the velocity pattern seen in Figures 2 and 3 suggests an inflow along the disk.

The above interpretation of the observed velocity structure was obtained by assuming the disk configuration, the gas motion along the disk plane, and the rotational axis parallel to the C–C′ cut. Nevertheless, if the rotational axis has a tilt from the cut direction, the pair of red and blue components in Figure 3 might be due to rotational motion (e.g., Keto 1990). To see whether this is the case, we made another two cuts through the center inclined from the C–C′ cut by ±12° (the axis of the bipolar outflow is inclined from the C–C′ cut by −12°) and found that the feature did not change as a whole. Therefore, if there is any tilt of the projected rotational axis from the C–C′ cut or not, the infall is necessary to form the pattern in Figure 3.

In the infall model, we assumed that the radial motion is along the disk plane. We now discuss another possibility: the observed velocity pattern is due to the motion perpendicular to the disk plane. In this case, the motion is interpreted to be outward contrary to the infall model, if we again assume the disk configuration. If the gas is dense part of the outflow [e.g., $\Delta V_{\rm outflow}$(CO) ~ 63 km s^{-1}; Snell et al. 1984], the projected velocity of the CS emission would be high and the gas would be accelerated as leaving the center for the outer region. However, the projected velocity of the radial motion is very small, ~(1–1.15) km s^{-1}; the small velocity width rather indicates a quiescent component, and the velocity tends to decrease as leaving the center in Figure 3. These features seem to be inconsistent with those expected of outflow (Snell et al. 1984). Kawabe et al. (1987) reported that CS(J = 2–1) spectrum averaged over a circular region with a 60″ diameter had a weak line wing emission with a ~20 km s^{-1}. It is this wing component that could be a part of the bipolar outflow.

Although the possibility of the contamination by the high velocity outflow cannot be totally ruled out, it is suggested that the radial motion of the gas is a flow going inward along the disk from the above discussions. To see how well the infall model fits the observed velocity patterns in Figures 2 and 3, we calculated position-velocity curves along the cuts based on a simple model: an infall of a constant velocity 1.5 km s^{-1} with a rigid rotation of r/8500 AU km s^{-1} in the inclined thin disk (assuming i = 60°). This simple infall model can reproduce the observed pattern in Figures 2 and 3. The slight difference between the observed velocity pattern and the model curve in Figure 3 would be caused by a decrease of infall velocity according to the distance from the center.

4.2. *Mass Estimation*

The lower limit of H_2 gas mass of the detected CS disk was estimated with the assumptions of LTE and an optically thin condition as

$$M(\mathrm{H_2}) = 4.1 \times 10^{-17} \frac{1}{X(\mathrm{CS})} \frac{\exp(2.4/T)}{1 - \exp(-4.7/T)} \times \left(\frac{D^2}{\mathrm{pc}^2}\right)\left(\frac{F_\nu \Delta V}{\mathrm{Jy\ km\ s^{-1}}}\right) M_\odot = 14 M_\odot , \quad (2)$$

where X (CS) is the abundance ratio of CS to H_2, T is the kinetic temperature in K, D is the distance to the CS source and assumed to be 900 pc (Harvey et al. 1979), and $F_\nu \Delta V$ is the total flux density integrated over the CS maps: 57 Jy km s^{-1}.

We adopt 10^{-9} for X(CS) according to the estimation by LVG model (Kawabe et al. 1987) and 29 K for T which was obtained by NH_3 $(J, K) = (1, 1)$ and $(2, 2)$ line observations (Takano 1986).

Free-free emission at 98 GHz is negligible: essentially all of the 98 GHz flux arises from dust, and the detected continuum flux density can be converted into H_2 mass of the dust disk. Since the present flux density at 98 GHz is highly similar to the result obtained at 110 GHz, we adopt the mass of 6–50 $M_\odot$ for the materials in the dust disk as estimated by Mundy & Adelman (1988).

Another approach is available for mass estimation. The lower limit of the mass existing in the region of $r \leq 8500$ AU including the stellar mass is evaluated to be 13 $M_\odot$, with the assumption of a rotational equilibrium at $r = 8500$ AU with the rotational velocity of 1 km s^{-1} (see Fig. 2 and its legend). This lower limit is compatible with the mass derived by the CS(2–1) and continuum flux density.

Most of the gas in the CS disk detected by our observation shows infall motion. The disk mass is ~ 14 $M_\odot$ with about 50% or more uncertainty owing to the uncertain physical quantities assumed in our estimation, e.g., D and X(CS). Accordingly, we assume that the gas mass in the central region going inward on spiral loci would be about 10 $M_\odot$ in the following discussion.

4.3. *Disk Accretion*

We discuss the physical nature of the disk accretion of dense molecular gas which is suggested from our observational results. The estimated infall velocity at several thousand AU scale is ~ 1.5 km s^{-1} as noted before. This is roughly consistent with a free-fall velocity in the gravitational potential of a central mass of ~ 20 $M_\odot$ including both the stellar mass (~ 6 $M_\odot$, as noted in the following) and the gas mass (~ 14 $M_\odot$). The dynamical time scale is estimated to be 8500 AU/1.5 km s^{-1} $\sim 3 \times 10^4$ yr, which is similar to the dynamical age of the CO bipolar outflow, 2×10^4 yr (Snell et al. 1984). Although these two time scales are different in kind, the coincidence might infer that disk accretion drives bipolar outflow. Mass infall rate in the disk is calculated to be $\sim 3 \times 10^{-4}$ $M_\odot$ yr^{-1}, using the estimated mass of accreting gas 10 $M_\odot$ and the dynamical time scale. The rate is much higher than that theoretically obtained for low-mass protostars, $c_s^3/G \sim 10^{-6}$ $M_\odot$ yr^{-1}, and such a high infall rate would make it possible to form a system of heavier protostar and associated disk.

The gas in the disk around the central star is spiraling inward due to a loss of angular momentum. An order-of-magnitude estimation of the loss rate of the angular momentum is possible by using $dL/dt \sim mrV_{\rm rot}/\delta t$. Assuming $m = 10$ $M_\odot$, $r = 8500$ AU, $V_{\rm rot} = 1$ km s^{-1}, and a time scale of the angular momentum loss $\delta t = 8500$ AU/1.5 km s^{-1} $\sim 3 \times 10^4$ yr, the required torque is calculated to be about 3×10^{44} ergs. Magnetic torque would be a possible candidate for removal of the angular momentum of the gas. Average field strength required to equal this torque is ~ 1 mG within a spherical volume of $r = 8500$ AU (Keto 1989). The local magnetic field in the vicinity of the GL 490 region was determined by near-infrared polarimetry (Hodapp 1990) to be almost perpendicular to the CO outflow axis; however, the field strength is yet unknown.

The infall rate obtained at the 8500 AU scale is so large that a rough estimation of accretion luminosity, $GM_{\rm ps}\dot{M}/r_{\rm ps}$, results in $\sim 10^4$ $L_\odot$ which is comparable to or rather larger than the bolometric luminosity of GL 490, $(1.4–2.7) \times 10^3$ $L_\odot$ (Harvey et al. 1979; Gear et al. 1985; Chini et al. 1991), where we assumed $r_{\rm ps} = 6$ $R_\odot$ (Stahler et al. 1980; Palla & Stahler 1990) $M_{\rm ps} = \dot{M} \times \tau_{\rm ps} \sim \dot{M} \times \tau_{\rm outflow}$ (Walker et al. 1986; Fukui et al. 1989), where $\tau_{\rm ps}$ and $\tau_{\rm outflow}$ is the age of the protostar and the bipolar outflow, 2×10^4 yr (Snell et al. 1984), respectively, and $\dot{M} = 3 \times 10^{-4}$ $M_\odot$ yr^{-1}, the "large-scale" infall rate. It could be suggested from the above estimation that GL 490 is a protostar which is luminous owing to the release of the gravitational energy of the gas accreting onto the star. However, the actual accretion rate at the stellar surface would be quite smaller, because not all mass is expected to reach the stellar surface (Cassen & Moosman 1981; Terebey et al. 1984), and also because the flow field could not be constant over five orders of magnitude in spatial scale. In this case, the central star should be at or near the ZAMS (Chini et al. 1991) and be luminous by itself, not by mass accretion.

We are grateful to Eric Keto for helpful comments. We thank the staff in the Nobeyama Radio Observatory for operation of the Nobeyama Millimeter Array. We also thank A. Rivkin for a careful reading of an earlier draft of the manuscript.

REFERENCES

Campbell, B., Persson, S. E., & McGregor, P. J. 1986, ApJ, 305, 336
Cassen, P., & Moosman, A. 1981, Icarus, 48, 353
Chikada, Y., et al. 1987, Proc. IEEE, 75, 1203
Chini, R., Henning, Th., & Pfau, W. 1991, A&A, 247, 157
Fukui, Y., Iwata, T., Takaba, H., Mizuno, A., Ogawa, H., Kawabata, K., & Sugitani, K. 1989, Nature, 342, 161
Gear, W. K., Gee, G., Robson, E. I., Ade, P. A. R., & Duncan, W. D. 1986, MNRAS, 219, 835
Harvey, P. M., Campbell, M. F., Hoffman, W. F., Thronson, H. A., & Gately, I. 1979, ApJ, 229, 990
Ho, P. T. P., and Haschick, A. D. 1986, ApJ, 304, 501
Hodapp, K.-W. 1990, ApJ, 352, 184
Ishizuki, S., Kawabe, R., Ishiguro, M., Okumura, S. K., Morita, K.-I., Chikada, Y., & Kasuga, T. 1990, Nature, 344, 224
Joyce, R. R., Capps, R. W., Gillett, F. C., Grasdalen, G., Kleinmann, S. G., & Sargent, D. G. 1977, ApJ, 312, L127
Kawabe, R., Hasegawa, T., Hayashi, S. S., & Kaifu, N. 1987, in IAU Symp. 115, Star Forming Regions, ed. M. Peimbert & J. Jugaku (Dordrecht: Reidel), 352
Kawabe, R., Ogawa, H., Fukui, Y., Takano, T., Takaba, H., Fujimoto, Y., Sugitani, K., & Fujimoto, M. 1984, ApJ, 282, L73
Keto, E. 1989, in IAU Symp. 120, Astrochemistry, ed. M. S. Vardya & S. P. Tarafdar (Dordrecht: Reidel), 122
———. 1990, in IAU Symp. 147, Fragmentation of Molecular Clouds and Star Formation, ed. E. Falgarone, F. Boulanger, & G. Duvert (Dordrecht: Reidel), 438
Lada, C. J., & Harvey, P. M. 1981, ApJ, 245, 58
Mundy, L. G., & Adelman, G. A. 1988, ApJ, 329, 907
Palla, F., & Stahler, S. W. 1990, ApJ, 360, L47
Persson, S. E., McGregor, P. J., & Campbell, B. 1988, ApJ, 326, 339
Snell, R. L., Scoville, N. Z., Sanders, D. B., & Erickson, N. R. 1984, ApJ, 284, 176
Stahler, S. W., Shu, F. H., & Taam, R. E. 1980, ApJ, 241, 637
Takano, T. 1986, ApJ, 303, 349
Terebey, S., Shu, F. H., & Cassen, P. 1984, ApJ, 286, 529
Walker, C. K., Lada, C. J., Young, E. T., Maloney, P. R., & Wilking, B. A. 1986, ApJ, 309, L47
Woody, D. P., Scott, S. L., Scoville, N. Z., Mundy, L. G., Sargent, A. I., Padin, S., Tinney, C. G., & Wilson, C. D. 1989, ApJ, 337, L41
Yamashita, T., Sato, S., Nagata, T., Gatley, I., Hayashi, S. S., & Fukui, Y. 1989, ApJ, 336, 832